# Flash-Quench Studies on the One-Electron Reduction of Triiodide

Byron H. Farnum, William M. Ward, and Gerald J. Meyer*

Departments of Chemistry and Materials Science & Engineering, Johns Hopkins University, 3400 North Charles Street, Baltimore, Maryland 21218, United States

ABSTRACT: The one-electron reduction of triiodide (I_3^-) by a series of reduced ruthenium polypyridyl compounds was studied in an acetonitrile solution at room temperature using the flash-quench technique. Reductive quenching of the metal-to-ligand charge-transfer excited state of $[Ru(bpy)_2(deeb)]^{2+}$, $[Ru(deeb)_2(bpy)]^{2+}$, or $[Ru(deeb)_3]^{2+}$, where bpy is 2,2′-bipyridine and deeb is 4,4′-$(CO_2CH_2CH_3)_2$-2,2′-bipyridine, by iodide generated the reduced ruthenium compounds and diiodide ($I_2^{\bullet-}$). Charge recombination of the reduced ruthenium compounds and $I_2^{\bullet-}$ occurred with rate constants near the calculated diffusion limit of 2.6×10^{10} M^{-1} s^{-1}. The reaction of the reduced ruthenium compounds with I_3^- was characterized spectroscopically through the addition of I_3^- into the experimental solution prior to the laser flash. Transient absorption data indicated that $I_2^{\bullet-}$ was a reaction product of I_3^- reduction and appeared with an average second-order rate constant of $(5.0 \pm 0.6) \times 10^9$ M^{-1} s^{-1} for all three compounds. The insensitivity of the rate constants for I_3^- reduction over an 80 meV change in the driving force was unexpected. The relevance of these findings to solar energy conversion within dye-sensitized solar cells is discussed.
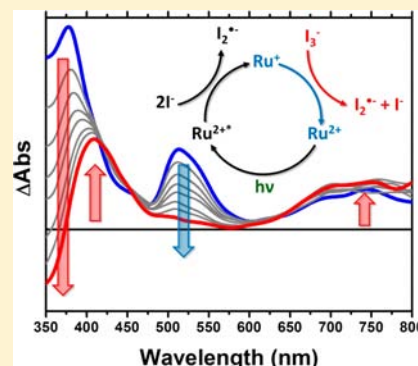

INTRODUCTION

Iodide/triiodide (I^-/I_3^-) continues to be the most widely used redox mediator for regenerative dye-sensitized solar cells (DSSCs).[1−3] Rapid regeneration of the oxidized sensitizer by iodide transfers the "hole" away from the injected electron and into solution. Triiodide is reduced at a platinum counter electrode to complete the circuit. Many alternative mediators accomplish rapid regeneration with high efficiency yet still yield poor solar energy conversion efficiencies because of unwanted recombination between the injected electrons, $TiO_2(e^-)$, and oxidized mediators.[2] In the case of I^-/I_3^-, the kinetics for recombination are quite slow, on the order of milliseconds at open circuit, and power conversion efficiencies greater than 10% often result.[2−4] The recombination mechanism and even the identity of the electron acceptor(s) remain speculative. While there are potentially many oxidized iodide species present in operational DSSCs, iodine (I_2) and triiodide are suspected of being the most likely acceptors. The recombination reaction is thought to be first-order in $TiO_2(e^-)$, often envisioned as Ti^{III} states, and first-order in the acceptor; therefore, eqs 1 and 2 describe the potential reactions with I_2 and I_3^-.[2,3]

$$TiO_2(e^-) + I_2 \rightarrow TiO_2 + I_2^{\bullet-} \tag{1}$$

$$TiO_2(e^-) + I_3^- \rightarrow TiO_2 + I_2^{\bullet-} + I^- \tag{2}$$
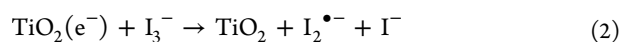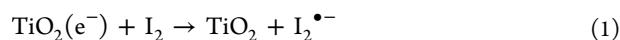
On the basis of the relevant equilibrium, eq 3, and a typical mediator solution composition of 0.5 M LiI/0.05 M I_2 in acetonitrile, the concentrations of I_2 and I_3^- in a DSSC are estimated to be 20 nM and 50 mM, respectively.[5] This calculation alone would appear to suggest that I_3^- is the only significant electron acceptor in the electrolyte solution.

However, previous studies have proposed that I_2 is the dominant acceptor, citing its low concentration as an explanation for slow recombination.[6,7] Regardless of which pathway is present, it is remarkable that a 50 mM concentration of triiodide does not facilitate the unwanted recombination reaction to the degree that major losses in efficiency are observed.

$$I^- + I_2 \rightleftharpoons I_3^- \qquad K_{eq}\,(CH_3CN) = 10^{6.7}\,M^{-1} \tag{3}$$
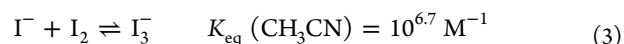
It remains unknown why I_3^- is able to escape the mesoporous TiO_2 thin film and reach the counter electrode effectively while avoiding recombination with $TiO_2(e^-)$. Stopped-flow and pulse radiolysis measurements in fluid solution have largely been limited to aqueous solvent, where the equilibrium in eq 3 is known to be vastly different from that in acetonitrile, $K_{eq}\,(H_2O) = 750\,M^{-1}$.[8−10] Conventional electrochemical methods are difficult because the reactivity of I^-/I_3^- is limited to $2e^-$ chemistry at most electrodes.[5,11,12] Recent photomodulated voltammetry measurements have provided experimental estimates of the $1e^-$ reduction potential for triiodide in acetonitrile and other solvents; however, there appears to be a large uncertainty in such measurements.[13,14]

In a recent paper, we reported the one-electron reduction of triiodide in acetonitrile using a flash-quench experiment.[15] The data provided the first spectroscopic evidence that diiodide ($I_2^{\bullet-}$) is indeed a reaction product, and an estimate of the $E°(I_3^-/I_2^{\bullet-})$ reduction potential was calculated. Here we expand on these earlier results and show generality in the reaction by providing two additional $1e^-$ reductants. An intimate mechanism for triiodide
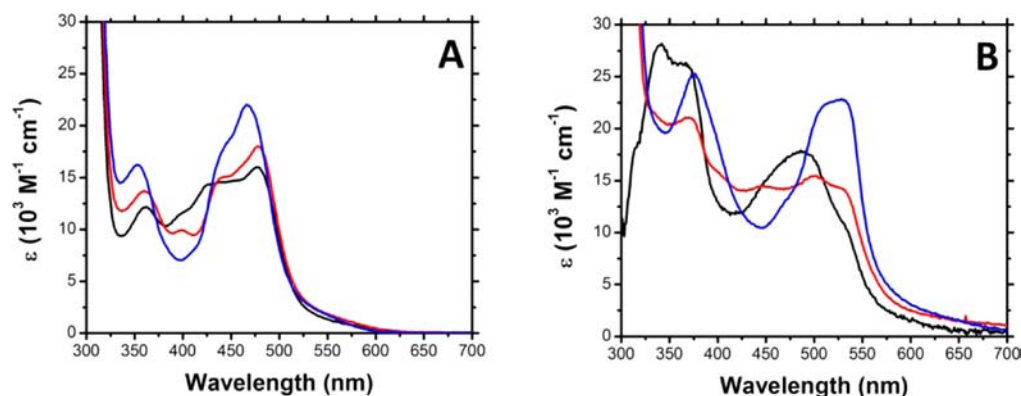
Figure 1. UV−vis extinction coefficient spectra of (A) Ru^{2+} and (B) Ru^+ for the compounds $[Ru(bpy)_2(deeb)]^{2+}$ (black), $[Ru(deeb)_2(bpy)]^{2+}$ (red), and $[Ru(deeb)_3]^{2+}$ (blue) in acetonitrile.

Table 1. Photophysical and Electrochemical Properties of the Ruthenium Polypyridyl Compounds[a]

	λ_{max}, nm (ε, M^{-1} cm^{-1})					$E°$ (V vs SCE)	
compound	Ru^{2+}	Ru^+	PL (nm)	τ (μs)	φ_{PL}	$Ru^{III/II}$	$Ru^{2+/+}$
$[Ru(bpy)_2(deeb)]^{2+}$	478 (16000)	488 (18000)	675	0.95	0.03	1.37	−1.00
$[Ru(deeb)_2(bpy)]^{2+}$	477 (18000)	500 (15000)	658	1.20	0.08	1.46	−0.98
$[Ru(deeb)_3]^{2+}$	467 (22000)	527 (23000)	630	2.10	0.13	1.56	−0.92

[a]All measurements in argon-saturated acetonitrile at room temperature.

reduction is proposed along with its relevance to the aforementioned recombination reaction.

EXPERIMENTAL SECTION

Materials. Argon gas (Mattson, 99.99%), $[Ru(bpy)_3]Cl_2 \cdot 6H_2O$ (Aldrich, 99.95%), tetrabutylammonium iodide (TBAI; Fluka, >99%), tetrabutylammonium triiodide (TBAI$_3$; Aldrich, ≥97%), triethylamine (TEA; Fisher, 99.9%), and acetonitrile (Burdick & Jackson, spectroscopic grade) were used as received without further purification. $[Ru(deeb)_2(bpy)](PF_6)_2$ was prepared by a literature method.[16] $[Ru(deeb)_3](PF_6)_2$ and $[Ru(bpy)_2(deeb)](PF_6)_2$ were available from previous studies.[17,18]

Measurements. *Steady-State Absorption.* UV−vis absorption spectra were obtained on a Varian Cary 50 UV−vis spectrophotometer at room temperature. The extinction coefficients for all ruthenium tris(diimine) compounds, Ru^{2+}, in argon-purged acetonitrile were determined spectroscopically through Beer's law analysis of solutions at known concentrations. The extinction coefficients for the one-electron-reduced compounds, Ru^+, were determined by generation of Ru^+ via steady-state photolysis of Ru^{2+} in the presence of 0.1 M TEA.[19]

Steady-State Photoluminescence (PL). A Spex fluorolog with a 450 W xenon lamp was utilized for steady-state PL measurements. PL spectra of Ru^{2+} compounds were acquired at room temperature in argon-purged acetonitrile. Comparative actinometry using $[Ru(bpy)_3]Cl_2$ in water was used to measure PL quantum yields.[20]

Electrochemistry. Cyclic voltammetry was measured using a BAS 50 electrochemical analyzer for solutions of the appropriate Ru^{2+} compound in 0.1 M TBAClO$_4$/acetonitrile at a scan rate of 100 mV/s. The three-electrode setup [glassy carbon disk (working electrode), platinum disk (counter electrode), Ag/AgCl (sat. KCl(aq)) (reference electrode)] was calibrated versus ferrocene (Fc$^{+/0}$) before and after all measurements. Half-wave potentials ($E_{1/2}$) were then corrected to the saturated calomel electrode (SCE) using $E°$(Fc$^{+/0}$) = 0.389 V vs SCE.

Nanosecond Transient Absorption/Time-Resolved PL. Argon-purged acetonitrile solutions of Ru^{2+} both with and without TBAI were excited by a pulsed Nd:YAG laser (BigSky Brilliant B, 8 ns fwhm, 1 Hz) tuned to 532 nm. A pulsed 150 W xenon arc lamp (Applied Photophysics) served as the probe beam for absorption measurements and was aligned perpendicularly to the laser excitation light. For time-resolved PL measurements, the white-light probe was blocked and the

sample was only exposed to 532 nm laser light. Detection was achieved with a monochromator (Spex 1702/04) optically coupled to an R928 photomultiplier tube (Hamamatsu). A 60-pulse average of the transient data was acquired on a computer-interfaced digital oscilloscope (LeCroy 9450, Dual 350 MHz). Laser fluence was monitored throughout and held constant at 10 mJ/pulse.

RESULTS

The UV−vis absorption, photoluminescence (PL), and electrochemical properties of $[Ru(bpy)_2(deeb)](PF_6)_2$, $[Ru(deeb)_2(bpy)](PF_6)_2$, and $[Ru(deeb)_3](PF_6)_2$, where bpy is 2,2′-bipyridine and deeb is 4,4′-(CO$_2$CH$_2$CH$_3$)$_2$-2,2′-bipyridine, were characterized in acetonitrile solvent at room temperature. The extinction coefficient spectra of Ru^{2+} and the reduced Ru^+ form of each compound are shown in Figure 1. The Ru^{2+} compounds displayed strong metal-to-ligand charge-transfer (MLCT) transitions in the 400−600 nm range. Excitation into these bands resulted in long-lived excited states with lifetimes (τ) in the range of 0.9−2.1 μs. Steady-state PL was observed to be broad and featureless at room temperature and blue-shifted as the number of deeb ligands around the metal center increased. A summary of the measured photophysical data is given in Table 1.

The electrochemical behavior for the series of compounds was consistent with that observed for ruthenium polypyridyl compounds in the literature.[21,22] For each compound, cyclic voltammetry in 0.1 M TBAClO$_4$/acetonitrile revealed a reversible $Ru^{III/II}$ wave at potentials more positive than 1.3 V vs SCE and three reversible ligand-based waves at potentials more negative than −0.9 V vs SCE. From comparisons of the photophysical and electrochemical data, it was determined that the first ligand-based reduction potential for each compound was always that of a deeb ligand. The reduction potentials for the metal-based, $Ru^{III/II}$, and deeb-based, $Ru^{2+/+}$, waves are presented in Table 1.

Pulsed laser excitation of Ru^{2+} in the presence of ∼10 mM TBAI resulted in nearly complete (>98%) quenching of excited-state molecules within 50 ns. Transient absorption features consistent with reduced Ru^+ and oxidized $I_2^{•−}$ appeared over the

same time scale. The standard addition of known extinction coefficient spectra of Ru^+ and $I_2^{\bullet-}$ (Figures 1 and 2, respectively)
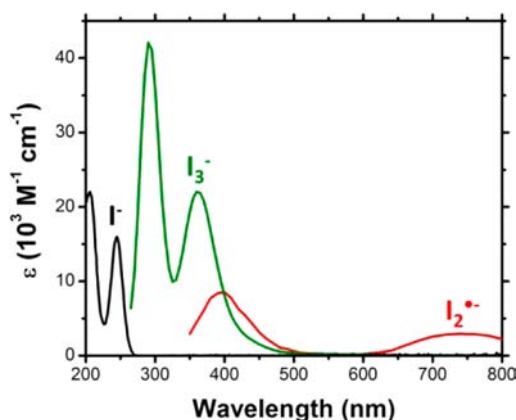

Figure 2. Extinction coefficient spectra for iodide (I^-), diiodide ($I_2^{\bullet-}$), and triiodide (I_3^-).
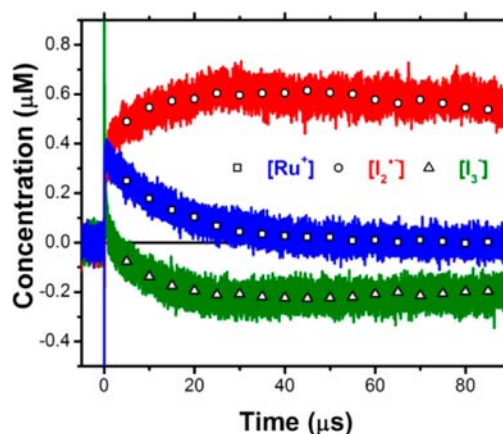

Figure 4. Concentration versus time plot that resulted from full-wavelength spectral modeling (open symbols) and selected wavelength matrix analysis (colored lines) of transient absorption features recorded for an acetonitrile solution that contained 26 μM $[Ru(deeb)_2(bpy)]^{2+}$, 8 mM I^-, and 15 μM I_3^-.

accurately simulated the transient absorption data and enabled their time-dependent concentrations to be calculated.

When $TBAI_3$ was added to solutions of similar composition, such as that above, transient absorption features around 500 nm, representative of Ru^+, decayed rapidly to baseline, while a transient bleach at 360 nm, representative of I_3^-, was observed over the same time range (Figure 3). At longer delay times, spectra resembled that of $I_2^{\bullet-}$ with positive features around 400 and 750 nm. Simulations of the transient data based on the extinction coefficient spectra of Ru^+, $I_2^{\bullet-}$, and I_3^- showed excellent agreement and gave no indication for the presence of additional light-absorbing species. From these simulations, the time-dependent concentration of each species was quantified.

Figure 4 shows a representative concentration versus time profile for the case of $[Ru(deeb)_2(bpy)]^{2+}$. The open-symbol data points were obtained from simulations of the full spectrum transient data, whereas the colored lines were calculated from matrix analysis discussed in detail below. Here it is important to note that the calculated concentrations for triiodide appeared as a change in the background concentration, $[I_3^-]_0$, and are therefore reported as $\Delta[I_3^-]$. From Figure 4, it is evident that $\Delta[I_3^-]$ and $[Ru^+]$ decreased concurrently over the first 30 μs, while the additional formation of $I_2^{\bullet-}$ occurred over the same time period, consistent

with I_3^- reduction by Ru^+ to yield $I_2^{\bullet-}$ as the product. On longer time scales than what is shown, $[I_2^{\bullet-}]$ and $\Delta[I_3^-]$ returned to the baseline with an equal second-order rate constant of 3×10^9 M^{-1} s^{-1}. This value was consistent with previous reports in the literature for the disproportionation of $I_2^{\bullet-}$ to yield I_3^- and I^-.[4,23] The UV−vis absorption spectra recorded before and after laser excitation revealed no evidence for permanent photochemistry.

To quantify the rate constant for the Ru^+ + I_3^- reaction, the initial triiodide concentration, $[I_3^-]_0$, was varied and transient absorption changes were monitored at selected wavelengths based on their principal importance to the transient species. For example, in the case of $[Ru(deeb)_2(bpy)]^{2+}$, 540 nm was chosen because Ru^+ is the primary light absorber at this wavelength. Additionally, 400 nm represented λ_{max} for $I_2^{\bullet-}$, and 360 nm was λ_{max} for I_3^-. At least three wavelengths were needed to fully quantify the relevant concentrations based on eq 4. Here $\Delta\varepsilon_\lambda^{Ru^+}$ is the difference in the extinction coefficients between Ru^+ and Ru^{2+} at a given wavelength and b is the path length.

$$\Delta Abs_\lambda(t)/b = \Delta\varepsilon_\lambda^{Ru^+}[Ru^+](t) + \varepsilon_\lambda^{I_2^{\bullet-}}[I_2^{\bullet-}](t) + \varepsilon_\lambda^{I_3^-}\Delta[I_3^-](t) \tag{4}$$
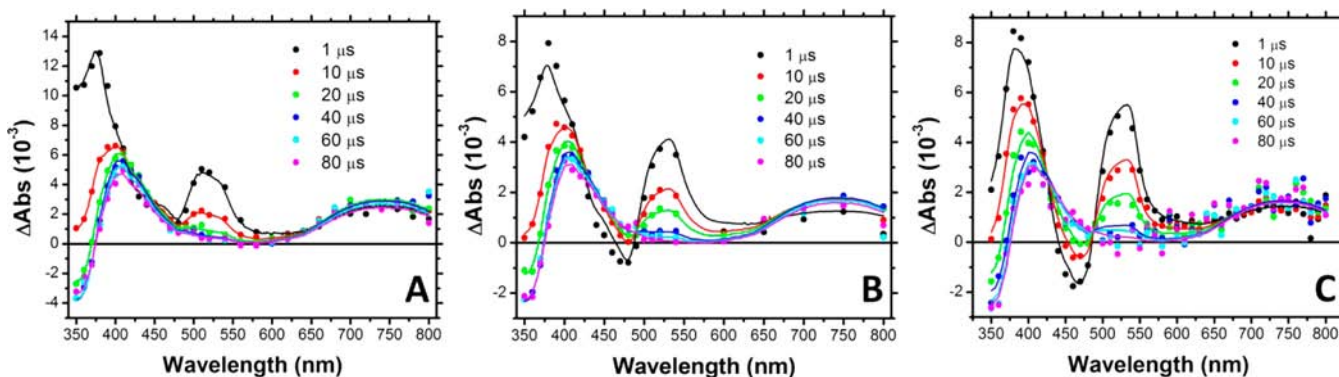

Figure 3. Transient absorbance difference spectra recorded at the indicated delay times after pulsed 532 nm laser excitation of an argon-purged acetonitrile solution that contained Ru^{2+}, I^-, and I_3^-. Solid lines are simulated spectra based on the standard addition of Ru^+, $I_2^{\bullet-}$, and I_3^- extinction coefficient spectra: (A) $[Ru(bpy)_2(deeb)]^{2+}$ = 35 μM, $[I^-]$ = 8 mM, $[I_3^-]$ = 15 μM; (B) $[Ru(deeb)_2(bpy)]^{2+}$ = 26 μM, $[I^-]$ = 8 mM, $[I_3^-]$ = 15 μM; (C) $[Ru(deeb)_3]^{2+}$ = 30 μM, $[I^-]$ = 8 mM, $[I_3^-]$ = 9 μM.

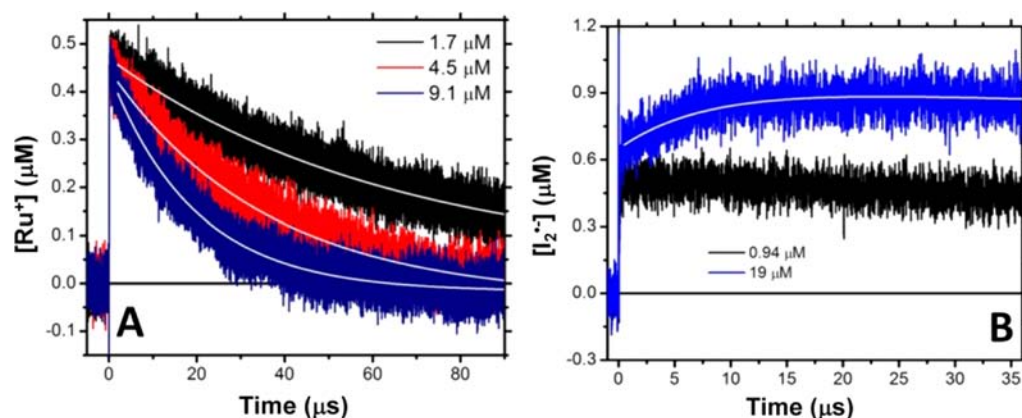**Figure 5.** Calculated concentration versus time curves in the case of $[Ru(deeb)_2(bpy)]^{2+}$ at the indicated $[I_3^-]_0$ for (A) $[Ru^+]$ and (B) $[I_2^{\bullet-}]$. Overlaid in white lines are pseudo-first-order kinetic fits.
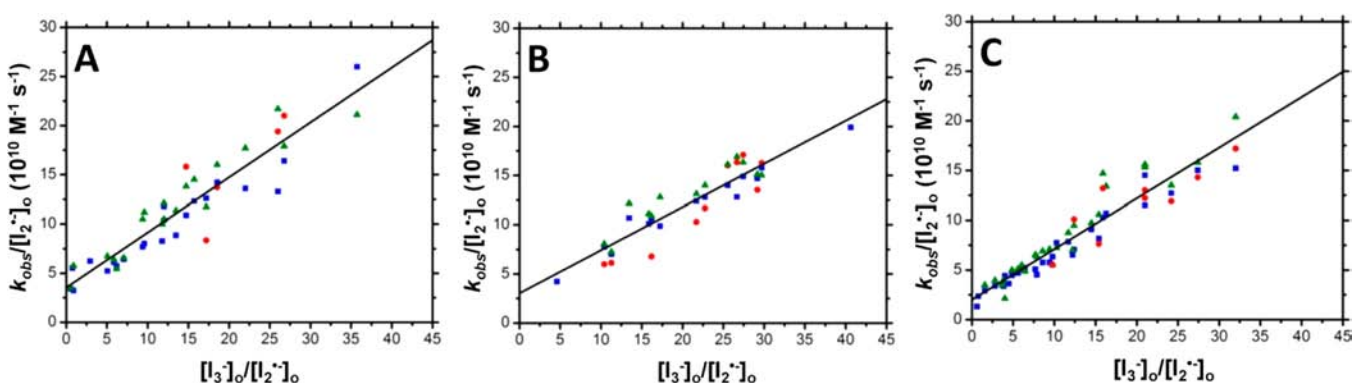

Figure 6. Plots of k_{obs} that correspond to $[Ru^+]$ decay (blue ■), $\Delta[I_3^-]$ decay (green ▲), and $[I_2^{\bullet-}]$ growth (red ●) for (A) $[Ru(bpy)_2(deeb)]^{2+}$, (B) $[Ru(deeb)_2(bpy)]^{2+}$, and (C) $[Ru(deeb)_3]^{2+}$. Data were fit collectively to the linear equation $k_{obs}/[I_2^{\bullet-}]_0 = k_2 + k_3[I_3^-]_0/[I_2^{\bullet-}]_0$.

Matrix analysis allowed for calculation of the concentration versus time data with respect to Ru^+, $I_2^{\bullet-}$, and I_3^-. The advantage to this method was that the same information obtained from full spectral analysis (open symbols in Figure 4) could be garnered from data collected at only three wavelengths. Matrix analysis was important because it enabled the loss of Ru^+ and I_3^- reactants to be correlated with the formation of $I_2^{\bullet-}$ products. This also greatly reduced the time required for the experiment and allowed a larger range of $[I_3^-]_0$ to be sampled. Equation 4 must be solved exactly and as a result the time dependent concentration data generally had poor signal-to-noise ratios relative to the absorption change. For this reason, an adjacent average smoothing was often applied to the concentration versus time data in order to match the observed signal-to-noise ratio.

Figure 5 shows the calculated $[Ru^+]$ as a function of time with increased $[I_3^-]_0$ for the case of $[Ru(deeb)_2(bpy)]^{2+}$. These data were well modeled by pseudo-first-order kinetics as a function of $[I_3^-]_0$. Time-dependent data for $\Delta[I_3^-]$ decay also followed a pseudo-first-order kinetic model at early time scales. Under low concentrations of $[I_3^-]_0$, the time-dependent $[I_2^{\bullet-}]$ concentration showed steady-state behavior over the time domain where $[Ru^+]$ and $\Delta[I_3^-]$ decreased. At higher $[I_3^-]_0$ concentrations, a pseudo-first-order growth of $[I_2^{\bullet-}]$ was resolved. When $[Ru^+]$ decayed to zero, the decay of $\Delta[I_3^-]$ and growth of $[I_2^{\bullet-}]$ reached a plateau and then began to return to the baseline via disproportionation of $I_2^{\bullet-}$.

The observed rate constants extracted from $[Ru^+]$, $[I_2^{\bullet-}]$, and $\Delta[I_3^-]$ data were related to the rate constant for recombination of Ru^+ with $I_2^{\bullet-}$, k_2, and the rate constant for I_3^- reduction, k_3, by the relation $k_{obs} = k_2[I_2^{\bullet-}] + k_3[I_3^-]$. A detailed description of this derivation is provided further in the Discussion section. Normalized plots of k_{obs} versus $[I_3^-]$ are shown in Figure 6 for the three compounds studied. The data on both axes were normalized to the initial concentration of $I_2^{\bullet-}$ formed after excited-state quenching, $[I_2^{\bullet-}]_0$. This allowed data from multiple experiments to be plotted together provided that $[I_2^{\bullet-}]$ changed very little over the fitted time domain. Second-order rate constants k_2 and k_3 obtained from linear fits of the data to the equation $k_{obs}/[I_2^{\bullet-}]_0 = k_2 + k_3[I_3^-]_0/[I_2^{\bullet-}]_0$ are given in Table 2.

Table 2. Second-Order Rate Constants for the Reaction of Ru^+ with $I_2^{\bullet-}$ (k_2) and I_3^- (k_3)[a]

| compound	k_2 (M^{-1} s^{-1})	k_3 (M^{-1} s^{-1})
$[Ru(deeb^-)(bpy)_2]^+$	$(3.5 \pm 0.5) \times 10^{10}$	$(5.6 \pm 0.3) \times 10^9$
$[Ru(deeb^-)(deeb)(bpy)]^+$	$(3.0 \pm 0.7) \times 10^{10}$	$(4.4 \pm 0.3) \times 10^9$
$[Ru(deeb^-)(deeb)_2]^+$	$(2.0 \pm 0.3) \times 10^{10}$	$(5.1 \pm 0.2) \times 10^9$

[a]Values given with a standard error.

■ DISCUSSION

Conventional flash-quench experiments have been utilized for some time now to study a wide variety of electron-transfer reactions.[24,25] This approach is particularly useful in the study of rapid kinetics, $k > 10^4$ s^{-1}. In a typical reductive flash-quench experiment, *flash* photolysis generates an excited state that is
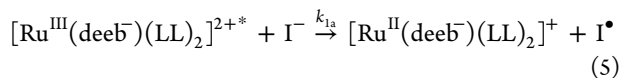
quenched by an electron donor, thus generating a reduced compound that can react with a species of interest. In the current study, three ruthenium polypyridyl compounds were utilized for their stability in the excited and reduced states, large extinction coefficients in the visible spectrum, and well-established outer-sphere electron-transfer chemistry.[21,22,26,27] Iodide and triiodide represented the donor and acceptor, respectively (Scheme 1). An

Scheme 1. Reductive Flash-Quench Cycle Where Ru²⁺ is the Chromophore, I⁻ is the Donor, and I₃⁻ is the Acceptor of Interest
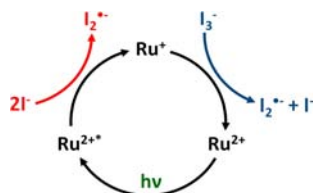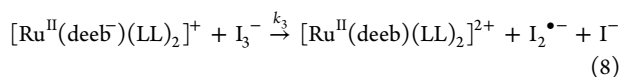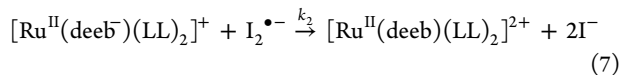

experimentally useful feature of this flash-quench assembly is that the excited state and thermal iodide redox chemistry ultimately yields ground-state products that enabled signal averaging after multiple laser pulses.

Mechanisms. Reductive quenching of $[Ru(bpy)_2(deeb)]^{2+*}$ and $[Ru(deeb)_3]^{2+*}$ by iodide in acetonitrile has been previously reported[17] and was shown to directly yield the reduced ruthenium compounds, abbreviated Ru^+, and $I^\bullet$ (eq 5) with $k_{1a} > 10^9$ M^{-1} s^{-1} for both excited state reactions. The formation of $I_2^{\bullet-}$ was observed as a secondary reaction product (eq 6) with a characteristic rate constant of $k_{1b} = 2.4 \times 10^{10}$ M^{-1} s^{-1}. Given the high concentration of iodide employed in the current study, the iodine atom was extremely short-lived and reacted to yield diiodide at the earliest time resolution. This same behavior was observed for all three compounds studied herein.

$$[Ru^{III}(deeb^-)(LL)_2]^{2+*} + I^- \xrightarrow{k_{1a}} [Ru^{II}(deeb^-)(LL)_2]^+ + I^\bullet \tag{5}$$

$$I^\bullet + I^- \xrightarrow{k_{1b}} I_2^{\bullet-} \tag{6}$$

The reaction of Ru^+ and I_3^- occurred in competition with the recombination of Ru^+ and $I_2^{\bullet-}$ (eqs 7 and 8). However, the I_3^- concentration was increased significantly such that the reaction of Ru^+ with I_3^- became the predominate electron-transfer pathway. Transient absorption spectroscopy clearly revealed that, as Ru^+ and I_3^- were consumed, $I_2^{\bullet-}$ was formed. When $[Ru^+]$ decayed to zero, disproportionation of $I_2^{\bullet-}$ (eq 9) could cleanly be observed as a loss of $[I_2^{\bullet-}]$ and growth of $\Delta[I_3^-]$ over time, $k_{dis} = 3 \times 10^9$ M^{-1} s^{-1}. The disproportionation reaction reset the concentrations of iodide and triiodide back to their initial values, as was confirmed by the fact that UV−vis absorption spectra recorded before and after laser excitation revealed no evidence for permanent photochemistry.

$$[Ru^{II}(deeb^-)(LL)_2]^+ + I_2^{\bullet-} \xrightarrow{k_2} [Ru^{II}(deeb)(LL)_2]^{2+} + 2I^- \tag{7}$$

$$[Ru^{II}(deeb^-)(LL)_2]^+ + I_3^- \xrightarrow{k_3} [Ru^{II}(deeb)(LL)_2]^{2+} + I_2^{\bullet-} + I^- \tag{8}$$

$$2I_2^{\bullet-} \xrightarrow{k_{dis}} I_3^- + I^- \tag{9}$$

The kinetics for $[Ru^+]$ decay were found to be pseudo-first-order, consistent with the integrated rate law (eq 10), where $k_{obs} = k_2[I_2^{\bullet-}] + k_3[I_3^-]$. The derivation of the rate law hinged on the assumption that $k_2[I_2^{\bullet-}] + k_3[I_3^-]$ remained constant throughout the decay of $[Ru^+]$. Calculation of k_{obs} at 1 and 30 μs for the data presented in Figure 4 and Table 2 revealed that k_{obs} changed less than 2% over this time range, despite the relative changes in the $[I_2^{\bullet-}]$ and $[I_3^-]$ concentrations. Therefore, for convenience, $k_{obs} = k_2[I_2^{\bullet-}] + k_3[I_3^-] = k_2[I_2^{\bullet-}]_0 + k_3[I_3^-]_0$, where $[I_2^{\bullet-}]_0$ is the concentration of diiodide initially formed by excited-state quenching and $[I_3^-]_0$ is the concentration of triiodide added to the solution.

$$[Ru^+]_t = [Ru^+]_0 e^{-k_{obs}t} \tag{10}$$

In the cases of $\Delta[I_3^-]$ decrease and $[I_2^{\bullet-}]$ growth, the differential rate laws were more complicated because of $I_2^{\bullet-}$ disproportionation. The corresponding integrated rate laws were complex and difficult to apply to the observed data. Pseudo-first-order rate laws similar to that of $[Ru^+]$ could be derived if disproportionation was ignored over the fitted time domain (eqs 11 and 12; see the Appendix for derivations). This assumption was valid when the $I_2^{\bullet-}$ concentration was kept small by operating at low laser power or when the concentration of I_3^- was high such that the growth of $I_2^{\bullet-}$ via I_3^- reduction was the dominant kinetic process.

$$\Delta[I_3^-]_t = \frac{k_3[I_3^-]_0[Ru^+]_0}{k_{obs}}(e^{-k_{obs}t} - 1) \tag{11}$$

$$[I_2^{\bullet-}]_t = [I_2^{\bullet-}]_0 + \frac{(k_{obs} - 2k_3[I_3^-]_0)[Ru^+]_0}{k_{obs}}(e^{-k_{obs}t} - 1) \tag{12}$$

Plots of $k_{obs}/[I_2^{\bullet-}]_0$ versus $[I_3^-]_0/[I_2^{\bullet-}]_0$ revealed self-consistent rate constants for $[Ru^+]$ and $\Delta[I_3^-]$ decay as well as $[I_2^{\bullet-}]$ growth. Of note is the fact that rate constants for $[I_2^{\bullet-}]$ growth were only obtained at $[I_3^-]_0/[I_2^{\bullet-}]_0$ ratios >10:1; this corresponded to roughly 70% of the Ru^+ molecules reacting with I_3^-. A linear fit of the compiled data resulted in an intercept equal to the second-order rate constant for recombination of Ru^+ and $I_2^{\bullet-}$ and a slope equal to the second-order rate constant for I_3^- reduction.

The rate constants for the reduction of $I_2^{\bullet-}$ were found to be fairly constant throughout the series of ruthenium polypyridyl compounds and similar to k_2 determined previously for $[Ru^{II}(bpz^-)(bpz)(deeb)]^+$ in the absence of I_3^-.[23] In fact, these reactions were determined to be diffusion-limited under the experimental conditions based on an estimate of $k_{diff} = 2.6 \times 10^{10}$ M^{-1} s^{-1} ($\mu = 8$ mM, acetonitrile).[15,28] Diffusion-limited kinetics are often observed for bimolecular electron-transfer reactions that occur with highly favorable $\Delta G°_{et}$.[21,29] Indeed, the recombination of Ru^+ and $I_2^{\bullet-}$ is expected to be strongly exergonic, $-\Delta G°_{et} > 1.5$ eV, and therefore the observed results are consistent with expectations based on previous literature reports.[3,30]

Intimate Mechanism for Triiodide Reduction. In the case of I_3^- reduction, electron transfer was formally from the π^* orbitals of the coordinated deeb ligand to the σ^* orbitals of I_3^-.[34] The rate constants obtained for the one-electron reduction of I_3^- were relatively constant throughout the series of ruthenium polypyridyl compounds, ranging from only 4.4×10^9 to 5.6×10^9 M^{-1} s^{-1}. Despite the narrow ~80 mV range of $E°(Ru^{2+/+})$ potentials examined, a stronger dependence on the

driving force was expected. With some assumptions, Marcus theory was previously applied to the I_3^- reduction data for $[Ru(deeb^-)(deeb)_2]^+$.[15] From this analysis, an estimate of $E°(I_3^-/I_2^{•-}) = -0.58$ V vs SCE was garnered that was close to values predicted in the literature.[3,15,30] On the basis of this previous calculation, rate constants for triiodide reduction were expected to be $\sim 10^{10}$ M^{-1} s^{-1} for $[Ru(deeb^-)(deeb)(bpy)]^+$ and $[Ru(deeb^-)(bpy)_2]^+$, but the values measured herein were significantly smaller. This unexpected insensitivity to the driving force results in at least an 80 mV uncertainty in our previously reported reduction potential. In addition, this provides some new insight into the possible mechanism and is therefore of interest to briefly discuss what led to such diminished experimental rate constants and their weak sensitivity to the driving force.

One possible explanation is that triiodide reduction was rate-limited by a mechanistic step prior to electron transfer. This putative step could reasonably be dissociation of I_3^- into I_2 and I^- after formation of an adduct with the reduced compound, followed by a rapid $Ru^+ + I_2$ reaction. In such a mechanism, diffusional encounters of I_3^- and Ru^+ generate an adduct that weakens the I−I bond and forms I_2, which rapidly undergoes $Ru^+ + I_2$ electron transfer. The reduction of molecular iodine is also expected to yield $I_2^{•-}$, and the driving force for this reaction is expected to be at least 0.4 eV more favorable than that for I_3^- reduction. Taken together, this supports a potentially slow I−I bond breaking of I_3^- followed by fast electron transfer.[3,5,30] The observed rate constant of such a composite reaction would then depend on both the I_3^- dissociation within the adduct and the electron-transfer rate constant; any driving force dependence may be masked by the adduct formation step. While the above mechanism cannot be ruled out, a mechanism where free iodine present in acetonitrile is directly reduced (eq 13) can reasonably be dismissed. A full derivation of this is given in the Appendix; however, simply stated, the concentration of free iodine is too small to account for the rapid reactivity that was observed. Rate constants of $k_4 \sim 10^{14}$ M^{-1} s^{-1} would need to be invoked to account for the observed data. Such rate constants are about 4 orders of magnitude larger than the expected diffusion limit. Therefore, the direct reduction of I_2 is not likely to be responsible for the observed kinetics.

$$[Ru^{II}(deeb^-)(LL)_2]^+ + I_2 \xrightarrow{k_4} [Ru^{II}(deeb)(LL)_2]^{2+} + I_2^{•-} \tag{13}$$
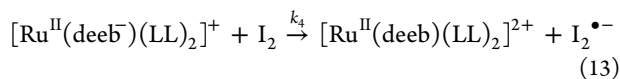
Another explanation is that triiodide reduction was limited by weak electronic coupling between Ru^+ and I_3^-. Semiclassical Marcus theory describes the electronic coupling between the donor and acceptor as a preexponential term, κ_{el} (eq 14), where ν_n is the nuclear frequency factor, often taken to be kT/h or 6.2×10^{12} s^{-1}, and $\Delta G^‡$ is the activation energy.[31,32]

$$k_{et} = \nu_n \kappa_{el} e^{-\Delta G^‡/RT} \tag{14}$$

To analyze this further, we estimated the electron-transfer rate constants for each ruthenium polypyridyl compound based on eq 15, where k_{diff} was reported above and the equilibrium association constant $K_A = 7$ M^{-1} ($\mu = 8$ mM, acetonitrile) was calculated from known expressions in the literature.[28,32,33] The result was $k_{et} = 1.0 \times 10^9$, 7.6×10^8, and 9.1×10^8 s^{-1} for $[Ru(deeb^-)(bpy)_2]^+$, $[Ru(deeb^-)(deeb)(bpy)]^+$, and $[Ru(deeb^-)(deeb)_2]^+$ respectively. The similarity in these values may suggest that $\Delta G^‡$ was small and that the reactions occurred on top of the Marcus curve; therefore, $k_{et} \sim \nu_n \kappa_{el}$. This estimation corresponded to $\kappa_{el} \sim 10^{-4}$. An electronic coupling constant of this magnitude

would indicate very little electronic overlap between Ru^+ and I_3^-. This may be accounted for in the poor symmetry alignment of the donor and acceptor orbitals, $\pi^*(deeb)$ and $\sigma^*(I_3^-)$, respectively.[34]

$$\frac{1}{k_3} = \frac{1}{k_{diff}} + \frac{1}{K_A k_{et}} \tag{15}$$

Further studies over a wider range of $E°(Ru^{2+/+})$ may give more insight into the 1e$^-$ reduction of triiodide. However, identification of appropriate ruthenium polypyridyl compounds for the flash-quench experiments with iodide is difficult. A useful compound must be both a long-lived excited-state oxidant, to efficiently react with iodide, and a strong reductant in the reduced state to react with triiodide. Further complications arise from the fact that Ru^+ reacts competitively with $I_2^{•-}$ and I_3^-. In principle, this can be mitigated by operating at high concentrations of I_3^-; however, the direct excitation of I_3^- often prevents the use of concentrations larger than 20 μM. With all of these considerations, we anticipate that excited states with lifetimes in excess of 100 ns and $E°(Ru^{2+*/+})$ reduction potentials greater than +1 V vs SCE will be useful for flash-quench studies of triiodide reduction in acetonitrile provided that the $E°(Ru^{2+/+})$ ground-state reduction potentials are more negative than -0.6 to -0.7 V vs SCE.

Relevance to DSSCs. The kinetics for recombination of injected electrons in TiO_2 with triiodide are known to be sluggish.[2−4,30] The data presented here show that the kinetics for molecular 1e$^-$ reductants were also limited, possibly by adduct formation or weak electronic overlap. Perhaps the same arguments can be made in the case of I_3^- reduction by $TiO_2(e^-)$, where an unfavorable surface association or poor overlap of the Ti^{III} frontier orbitals and those of I_3^- lead to slow kinetics. $\Delta G°$ for the recombination reaction is also unknown given that the density of states for the TiO_2 conduction band tails exponentially to lower energies.[2,35] The trapped Ti^{III} states are known to be present at these lower energies, therefore limiting their thermodynamic capacity for triiodide reduction.

The slow recombination kinetics in DSSCs have also been attributed to I_2 reduction as the main pathway.[6,7] This mechanism cites the expected low concentration of I_2 present in the cell as the reason for slow reactivity. We considered this mechanism as an explanation for the observed rate constants for triiodide reduction. This resulted in a rate constant for I_2 reduction by Ru^+ that was beyond the diffusion limit. Therefore, I_2 reduction was unlikely in these flash-quench experiments.

The reduction of triiodide by ruthenium polypyridyl compounds is directly relevant to p-type DSSCs. In this type of solar cell, the accepted mechanism is as follows: light absorption creates an excited state followed by "hole" transfer to the semiconductor, usually NiO, thus yielding a reduced sensitizer[14] that is regenerated by 1e$^-$ transfer to I_3^-.[36−38] To date, p-type DSSCs have notoriously poor power conversion efficiencies in comparison to the more widely studied n-type DSSCs. The interfacial recombination of semiconductor holes with reduced sensitizers has been cited as the major reason for such low efficiencies. This process occurs rapidly on the picosecond time scale; therefore, in order to generate an appreciable photocurrent, sensitizer regeneration by I_3^- needs to occur on a similar time scale.[14,39] Indeed, Morandeira et al. have shown that I_3^- reduction by a reduced coumarin 343 sensitizer on NiO occurs rapidly; however, a majority of reduced sensitizers were still found to recombine with NiO holes.[39] The results presented here indicate that electron transfer from reduced ruthenium polypyridyl sensitizers to triiodide may not be able to effectively compete with interfacial recombination to semiconductor holes.

■ CONCLUSION

In summary, we have reported compelling evidence that $I_2^{\bullet-}$ is a product of the $1e^-$ reduction of I_3^- in acetonitrile. The rate constants for the electron-transfer reaction were determined for three reduced ruthenium polypyridyl compounds and were approximately independent of the free-energy change over an ~80 meV range. The insensitivity of the reaction to the driving force may reflect a slow dissociative step that precedes electron transfer and/or an electron-transfer event that occurs near the top of the Marcus curve. These findings have implications for solar energy conversion with I^-/I_3^- redox mediators. For example, the reduction of I_3^- yields a $I_2^{\bullet-}$ product that is more easily reduced and could potentially accept a second electron. On the other hand, $I_2^{\bullet-}$ undergoes rapid disproportionation to yield two products that are not easily reduced, I^- and I_3^-. This suggests that alternative redox mediators where the donor oxidation initiates a rapid disproportionation reaction to yield products that are not easily reduced will also result in high-efficiency DSSCs.
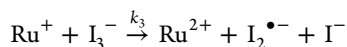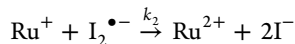
■ APPENDIX

Kinetic Derivations I. Triiodide Reduction

Assumptions and Definitions. (i) Excited-state quenching was complete within 10 ns, corresponding with the instrument response time.

(ii) Disproportionation of $I_2^{\bullet-}$ was considered to be insignificant within the time frame of Ru^+ decay.

(iii) The sum of $k_2[I_2^{\bullet-}] + k_3[I^{3-}]$ was a constant throughout the fitted time range. Therefore, $k_2[I_2^{\bullet-}] + k_3[I^{3-}] = k_2[I_2^{\bullet-}]_0 + k_3[I^{3-}]_0$.

Mechanism.

$$Ru^+ + I_2^{\bullet-} \xrightarrow{k_2} Ru^{2+} + 2I^-$$

$$Ru^+ + I_3^- \xrightarrow{k_3} Ru^{2+} + I_2^{\bullet-} + I^-$$

Rate Laws. $[Ru^+]$

$$-\frac{d[Ru^+]}{dt} = (k_2[I_2^{\bullet-}]_0 + k_3[I_3^-]_0)[Ru^+] = k_{obs}[Ru^+]$$

Integrating...

$$[Ru^+]_t = [Ru^+]_0 e^{-k_{obs}t}$$

$$[I_2^{\bullet-}]$$

$$-\frac{d[I_2^{\bullet-}]}{dt} = (k_2[I_2^{\bullet-}]_0 - k_3[I_3^-]_0)[Ru^+]$$

$$= (k_{obs} - 2k_3[I_3^-]_0)[Ru^+]_0 e^{-k_{obs}t}$$

Integrating...

$$[I_2^{\bullet-}]_t = [I_2^{\bullet-}]_0 + \frac{(k_{obs} - 2k_3[I_3^-]_0)[Ru^+]_0}{k_{obs}}(e^{-k_{obs}t} - 1)$$

$$[I_3^-]$$

$$-\frac{d[I_3^-]}{dt} = -\left(\frac{d\Delta[I_3^-]}{dt} + \frac{d[I_3^-]_0}{dt}\right) = -\frac{d\Delta[I_3^-]}{dt}$$

$$-\frac{d\Delta[I_3^-]}{dt} = k_3[I_3^-]_0[Ru^+] = k_3[I_3^-]_0[Ru^+]_0 e^{-k_{obs}t}$$
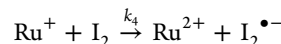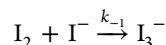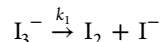
Integrating...

$$\Delta[I_3^-]_t = \frac{k_3[I_3^-]_0[Ru^+]_0}{k_{obs}}(e^{-k_{obs}t} - 1)$$

Kinetic Derivations II. Iodine Reduction

Assumptions and Definitions. (i) Steady-state approximation for $[I_2]$. (ii) $K_{eq} = k_{-1}/k_1$.

Mechanism.

$$I_3^- \xrightarrow{k_1} I_2 + I^-$$

$$I_2 + I^- \xrightarrow{k_{-1}} I_3^-$$

$$Ru^+ + I_2 \xrightarrow{k_4} Ru^{2+} + I_2^{\bullet-}$$

Steady-State Approximation. $[I_2]$

$$-\frac{d[I_2]_{ss}}{dt} = k_{-1}[I_2]_{ss}[I^-] - k_1[I_3^-]_0 + k_4[I_2]_{ss}[Ru^+] = 0$$

$$[I_2]_{ss} = \frac{k_1[I_3^-]_0}{k_{-1}[I^-] + k_4[Ru^+]} \qquad \text{where } k_{-1}[I^-] \gg k_4[Ru^+]$$

$$[I_2]_{ss} = \frac{[I_3^-]_0}{K_{eq}[I^-]} \qquad \text{where } k_4 = k_3 K_{eq}[I^-]_0$$

Rate Laws. $[Ru^+]$

$$-\frac{d[Ru^+]}{dt} = (k_2[I_2^{\bullet-}]_0 + k_4[I_2]_{ss})[Ru^+]$$

$$= \left(k_2[I_2^{\bullet-}]_0 + \frac{k_4}{K_{eq}[I^-]}[I_3^-]_0\right)[Ru^+]$$

■ AUTHOR INFORMATION

Corresponding Author
*E-mail: meyer@jhu.edu.

Notes
The authors declare no competing financial interest.

■ ACKNOWLEDGMENTS

■ REFERENCES

(1) O'Regan, B.; Grätzel, M. *Nature* **1991**, *353*, 737−740.
(2) Ardo, S.; Meyer, G. J. *Chem. Soc. Rev.* **2009**, *38*, 115−164.
(3) Boschloo, G.; Hagfeldt, A. *Acc. Chem. Res.* **2009**, *42*, 1819−1826.
(4) Rowley, J.; Meyer, G. J. *J. Phys. Chem. C* **2009**, *113*, 18444−18447.
(5) Datta, J.; Bhattacharya, A.; Kundu, K. K. *Bull. Chem. Soc. Jpn.* **1988**, *61*, 1735−1742.
(6) Green, A. N. M.; Chandler, R. E.; Haque, S. A.; Nelson, J.; Durrant, J. R. *J. Phys. Chem. B* **2005**, *109*, 142−150.
(7) O'Regan, B. C.; Walley, K.; Juozapavicius, M.; Anderson, A.; Matar, F.; Ghaddar, T.; Zakeeruddin, S.; Klein, C.; Durrant, J. R. *J. Am. Chem. Soc.* **2009**, *131*, 3541−3548.
(8) Schwarz, H. A.; Bielski, B. H. J. *J. Phys. Chem.* **1986**, *90*, 1445−1448.
(9) Sun, J.; Stanbury, D. M. *Inorg. Chem.* **1998**, *37*, 1257−1263.

(10) Treinin, A.; Hayon, E. *Int. J. Radiat. Phys. Chem.* **1975**, *7*, 387−393.

(11) *Encyclopedia of Electrochemistry of the Elements*; Bard, A. J., Ed.; Marcel Dekker Inc.: New York, 1973; Vol. *1*.

(12) Oskam, G.; Bergeron, B. V.; Meyer, G. J.; Searson, P. C. *J. Phys. Chem. B* **2001**, *105*, 6867−6873.

(13) Boschloo, G.; Gibson, E. A.; Hagfeldt, A. *J. Phys. Chem. Lett.* **2011**, *2*, 3016−3020.

(14) Gibson, E. A.; Le Pleux, L.; Fortage, J.; Pellegrin, Y.; Blart, E.; Odobel, F.; Hagfeldt, A.; Boschloo, G. *Langmuir* **2012**, *28*, 6485−6493.

(15) Farnum, B. H.; Gardner, J. M.; Meyer, G. J. *Inorg. Chem.* **2010**, *49*.

(16) Bergeron, B. V.; Meyer, G. J. *J. Phys. Chem. B* **2003**, *107*, 245−254.

(17) Farnum, B. H.; Jou, J. J.; Meyer, G. J. *Proc. Natl. Acad. Sci. U.S.A.* **2012**, PNAS Early Edition, doi: 10.1073/pnas.1118340109.

(18) Marton, A.; Clark, C. C.; Srinivasan, R.; Freundlich, R. E.; Narducci Sarjeant, A. A.; Meyer, G. J. *Inorg. Chem.* **2006**, *45*, 362−369.

(19) Crutchley, R. J.; Lever, A. B. P. *J. Am. Chem. Soc.* **1980**, *102*, 7128−7129.

(20) Demas, J. N.; Addington, J. W. *J. Am. Chem. Soc.* **1976**, *98*, 5800−5806.

(21) Juris, A.; Balzani, V.; Barigelletti, F.; Campagna, S.; Belser, P.; Von Zelewsky, A. *Coord. Chem. Rev.* **1988**, *84*, 85−277.

(22) Rillema, D. P.; Allen, G.; Meyer, T. J.; Conrad, D. *Inorg. Chem.* **1983**, *22*, 1617−1622.

(23) Gardner, J. M.; Abrahamsson, M.; Farnum, B. H.; Meyer, G. J. *J. Am. Chem. Soc.* **2009**, *131*, 16206−16214.

(24) Chang, I.; Gray, H. B.; Winkler, J. R. *J. Am. Chem. Soc.* **1991**, *113*, 7056−7057.

(25) Dempsey, J. L.; Winkler, J. R.; Gray, H. B. *J. Am. Chem. Soc.* **2010**, *132*, 1060−1065.

(26) Allen, G. H.; White, R. P.; Rillema, D. P.; Meyer, T. J. *J. Am. Chem. Soc.* **1984**, *106*, 2613−2620.

(27) Sutin, N.; Creutz, C. *Adv. Chem. Ser.* **1978**.

(28) Steinfeld, J. L.; Francisco, J. S.; Hase, W. L. *Chemical Kinetics and Dynamics*; Prentice Hall: New York, 1989.

(29) Hug, G. L.; Marciniak, B. *J. Phys. Chem.* **1995**, *99*, 1478−1483.

(30) Rowley, J. G.; Farnum, B. H.; Ardo, S.; Meyer, G. J. *J. Phys. Chem. Lett.* **2010**, *1*, 3132−3140.

(31) Marcus, R. A.; Sutin, N. *Biochim. Biophys. Acta* **1985**, *811*, 265−322.

(32) Sutin, N. *Acc. Chem. Res.* **1982**, *15*, 275−282.

(33) Morel, F. M. M.; Hering, J. G. *Principles and Applications of Aquatic Chemistry*; John Wiley and Sons, Inc.: New York, 1993.

(34) Choi, H.; Bise, R.; Hoops, A. A.; Neumark, D. M. *J. Chem. Phys.* **2000**, *113*, 2255−2262.

(35) Fabregat-Santiago, F.; Mora-Sero, I.; Garcia-Belmonte, G.; Bisquert, J. *J. Phys. Chem. B* **2003**, *107*, 758−768.

(36) Lepleux, L.; Chavillon, B.; Pellegrin, Y.; Blart, E.; Cario, L.; Jobic, S.; Odobel, F. *Inorg. Chem.* **2009**, *48*, 8245−8250.

(37) Zhu, H.; Hagfeldt, A.; Boschloo, G. *J. Phys. Chem. C* **2007**, *111*, 17455−17458.

(38) Mori, S.; Fukuda, S.; Sumikura, S.; Takeda, Y.; Tamaki, Y.; Suzuki, E.; Abe, T. *J. Phys. Chem. C* **2008**, *112*, 16134−16139.

(39) Morandeira, A.; Boschloo, G.; Hagfeldt, A.; Hammarström, L. *J. Phys. Chem. C* **2008**, *112*, 9530−9537.